# Circular Dichroic Investigation of the Native and Non-native Conformational States of the Growth Factor Receptor-Binding Protein 2 N-Terminal *src* Homology Domain 3: Effect of Binding to a Proline-rich Peptide from Guanine Nucleotide Exchange Factor†

J. A. Bousquet,*,‡ C. Garbay,§ B. P. Roques,§ and Y. Mély‡

*Pharmacologie et Physico-Chimie des Interactions Cellulaires et Moléculaires, UMR CNRS 7034, Faculté de Pharmacie de Strasbourg, Université Louis Pasteur, BP 24, F-67401 Illkirch, France, and Département de Pharmacochimie Moléculaire et Structurale, INSERM U 266−UMR CNRS 8600, UFR des Sciences Pharmaceutiques et Biologiques, Université René Descartes, 4 Avenue de l'Observatoire, 75270 Paris Cedex 06, France*

*Received December 20, 1999; Revised Manuscript Received April 6, 2000*

ABSTRACT: SH3 (*src* homology domain 3) domains are small protein modules that interact with proline-rich peptides. The structure of the N-terminal SH3 domain from growth factor receptor-binding protein 2 (Grb2), an adapter protein in the intracellular signaling pathway to Ras, was investigated by circular dichroic (CD) spectroscopy. The compact native $\beta$-barrel conformation, previously elucidated by NMR spectroscopy, was largely predominant at pH = 4.8, in the absence of salt. From the structural changes induced by varying pH, ionic strength, temperature, or hydrophobicity of the environment, evidence for the existence of distinct nonnative conformations was obtained in the far- and near-UV domains. Along the free energy scale, these appear to distribute into two conformational ensembles, depending on the extent of structural and thermodynamic differences compared to the native conformation. The first ensemble consists of non-native conformations with a nativelike secondary structure, and the second is composed of partially unfolded conformations having short α-helical fragments or turnlike motifs in their nonnative secondary structure. Most of the observed nonnative conformations exist in mild or nondenaturing conditions. They probably have distinct compactness of their inner structure, depending on the strength of nonlocal interactions, but only the native all-$\beta$ conformation possesses a condensed protein exterior, appropriate for the binding to the VPPPVPPRRR decapeptide from Sos. Upon binding, the native conformation undergoes a local tertiary structure change in a hydrophobic pocket at the binding site. This is accompanied by the PP-II helix folding of the proline-rich peptide. Interestingly, in the near-UV domain, a significant change in the spectral contribution of an aromatic exciton was observed, thus allowing quantitative tracking of the binding process.

The growth factor receptor-binding protein 2 (Grb2)[1] is a ubiquitously expressed triple-domain protein, consisting of a single SH2 domain (Src homology domain 2) flanked by two SH3 domains. Grb2 is an adapter protein that binds to a proline-rich region of the C-terminal tail of Sos (Son of sevenless), the guanine nucleotide exchange factor of Ras (*1*), via both SH3 domains. As well, by its SH2 domain, Grb2 recognizes phosphotyrosine residues of stimulated receptors. Thus, upon activation and subsequent autophosphorylation of specific tyrosine residues, the epidermal growth factor (EGF) receptor is able to directly or indirectly (via Shc, another tyrosine-phosphorylated protein responding to cell stimulation) recruit the Grb2/Sos complex near the plasma membrane. The kinase cascade in the Ras/MAP signaling pathway then relays the signal to the nucleus, thereby allowing control of cell growth and differentiation (*2*).

SH3 domains are small protein modules (approximately 60 amino acids) first identified in Src (*3*) and spectrin (*4*). Investigation of several SH3 domains has revealed the conserved structural features of these single-domain protein modules (see ref *5* for a review). The SH3 fold consists of two small antiparallel $\beta$-sheets packing against each other in a sandwich form. A set of conserved residues on the protein surface binds to ligands containing proline-rich regions (PxxP motifs) (*6*), allowing SH3 domains to mediate cytoplasmic protein−protein recognition in eukaryotic signaling pathway (*7*) or in interactions involving cytoskeletal proteins (*8*).

The structure of the SH3 domain from the N-terminal part of Grb2 (56 amino acids) has been elucidated by NMR (*9*−

† This work was supported by the Ligue Nationale Contre le Cancer (Commité de Paris), Université Louis Pasteur, and the CNRS.

* Corresponding author: Tel (33) 03 88 67 69 98; fax (33) 03 88 67 40 11; e-mail bousquet@pharma.u-strasbg.fr.

‡ Université Louis Pasteur.

§ Université René Descartes.

[1] Abbreviations: Grb2, growth factor receptor-binding protein 2; SH3, *src* homology domain 3; Sos, guanine nucleotide exchange factor; CD, circular dichroism; NOE, nuclear Overhauser enhancement; C32S, single mutant of the growth factor receptor-binding protein 2 N-terminal *src* homology domain 3, in which Cys32 was replaced by Ser; Y7V/C32S, double mutant in which Tyr7 residue was additionally replaced by Val.

10.1021/bi9929103 CCC: $19.00 
Published on Web 06/08/2000

*11*). The folded conformation at acidic pH is formed from six $\beta$-strands distributed in two orthogonal antiparallel $\beta$-sheets. These $\beta$-sheets are three-stranded, sharing a bent $\beta$-strand, that yields a $\beta$-barrel-like structure. The overall structure is stabilized by numerous hydrophobic interactions. The conserved aromatic residues gather on the top edge of the protein, forming a smooth platform bordered by loops containing acidic residues. This external region constitutes most of the peptide binding site and has two hydrophobic pockets that interact with the protruding side chains in the proline-rich motif.

We report here a CD investigation, in the far- and near-UV domains, of the native conformation of Ser-32-Grb2-N-SH3, an oxidation-resistant mutant of the N-terminal SH3 domain of Grb2. The results were first satisfactorily compared to those obtained previously by NMR spectroscopy. Then, different experimental conditions were used, with pH, ionic strength, temperature, or hydrophobicity of the environment being varied, as well as by use of denaturing agents. Evidence for distinct nonnative interconverting conformations of the SH3 domain was obtained. Finally, we also analyzed the structural changes in both the SH3 domain and the proline-rich VPPPVPPRRR decapeptide upon binding. CD spectroscopy proved to be useful for readily bringing out information about the overall and local structural features of the SH3 domain, either isolated or complexed.

## MATERIALS AND METHODS

*Materials*. Ser-32-Grb2-N-SH3 and the proline-rich decapeptide VPPPVPPRRR were prepared by solid-phase synthesis, as previously reported (*9*). All chemicals were reagent-grade. Urea and guanidine hydrochloride were from Serva, and trifluoroethanol and sodium dodecyl sulfate were from Sigma. Phosphate buffers (10 mM), at a given pH, were prepared from a mixture of monopotassium phosphate and disodium phosphate (Merck), the final pH value being adjusted with diluted HCl solutions.

*Circular Dichroism*. CD spectra were recorded on a Jobin-Yvon CD VI nitrogen-flushed dichrograph fitted with a thermostated cell holder interfaced with a temperature-controlled water bath. Protein concentration of the samples ranged between $5 \times 10^{-7}$ and $5 \times 10^{-6}$ M for measurements in the far-UV domain and was $(2 \pm 0.5) \times 10^{-5}$ M for measurements in the near-UV domain. Cell path lengths of 0.02, 0.1, or 0.2 cm were used in the far-UV domain and a 1 cm cell path length was used in the near-UV domain. Calibration was done with (+)-camphorsulfonic acid ($\Delta\epsilon_{290.5nm} = 2.37\ M^{-1}\ cm^{-1}$ and $\Delta\epsilon_{192.5nm} = -4.95\ M^{-1}\ cm^{-1}$) (*12*). Temperature was controlled at $20 \pm 0.2$ °C for all experiments, unless otherwise mentioned. Spectra were acquired by averaging 4, 9, or 16 scans and corrected for buffer signal. To estimate the secondary structure contents, the Provencher procedure, using the CONTIN program, was usually applied (*13*). This estimation generally gives a reliable value of $\alpha$-helix content, provided that far-UV absorption bands due to chromophoric groups such as aromatic side chains or disulfide bridges do not overlap those of peptide bonds or couple with them in an asymmetric environment (*14*). Regarding $\beta$-structure, a single value is obtained, and the various types of $\beta$-structures such as $\beta$-sheets (parallel and antiparallel), $\beta$-hairpins, or $\beta$-turns are not discriminated. Thus, to get an estimate of irregular structures such as $\beta$-turns, the Johnson variable selection method was applied (*15*), with a wavelength interval of 0.5 nm for scanning spectra. Units of molecular ellipticity (deg·cm$^2$·dmol$^{-1}$) are per backbone amide in the far-UV range and per aromatic residue in the near-UV range. For denaturation measurements, samples were allowed to equilibrate for 15 min with the denaturant before spectra were recorded. As the molecular ellipticity of the native and completely unfolded states were found to not significantly depend on denaturant concentration in the pre- and posttransition regions, no correction for curve sloping was applied. In heating experiments, the enthalpy at the midpoint temperature, $\Delta H(T_M)$, was calculated from the van't Hoff equation: $d \ln K/dT = \Delta H/RT^2$.

*Correction for the Binding Affinity Measurement*. As the binding of the native all-$\beta$ conformation for the proline-rich peptide was evaluated in conditions where the native conformation is mainly exchanging with the $\alpha/\beta$ conformation, the measured binding constant is an apparent one. Moreover, the binding of the proline-rich peptide is expected to induce a substantial shift of the involved equilibrium:

$$I \overset{K_1}{\rightleftharpoons} N + P \overset{K_a}{\rightleftharpoons} C \qquad (1)$$

where I and N are the free $\alpha/\beta$ and native all-$\beta$ conformations, respectively, while P is the free decapeptide and C is the complex formed from the bound decapeptide and the SH3 domain. $K_1$ is the equilibrium constant in solution, and $K_a$ is the binding affinity of the all-$\beta$ conformation for the decapeptide. In this respect, the relationship between $K_a$ and the measured affinity, $K_{app}$, can be expressed as

$$K_a = K_{app}(1 + K_1)/K_1 \qquad (2)$$

For example, at neutral pH, where the concentrations of the native all-$\beta$ and the $\alpha/\beta$ conformations are nearly equal, $K_a \approx 2K_{app}$.

## RESULTS

*Effect of pH on CD Structure*. The secondary structure of the mutant Ser-32-Grb2-N-SH3 was analyzed by circular dichroism spectroscopy for pH values between 2 and 12, in the absence of salt. Significant changes in the entire far-UV profile of the SH3 domain were observed as a function of pH. The normalized amplitudes of molecular ellipticity were plotted versus pH, at various critical wavelengths (Figure 1A). This allows us to distinguish pH domains in which the CD signals do not significantly vary. These domains are separated by single transitions and were associated with distinct estimations of secondary structure content of the SH3 domain (Figure 1B) and far-UV CD spectra (Figure 2).

Only the transition centered at near-neutral pH (transition II) is completely reversible. It likely separates two distinct protein conformations. The existence of the first conformation at pH 4−6 is shown by the presence of a plateau in the CD signals (Figure 1A) and the estimated secondary structure content (Figure 1B). The corresponding flat CD spectrum at pH = 4.8 (Figure 2) exhibits low-amplitude broad bands. The positive molecular ellipticity (2600 deg·cm$^2$·dmol$^{-1}$) at the maximum intensity near 195 nm, coupled with a negative value of similar intensity at the smooth minimum about 215 nm, are typical of a nontwisted antiparallel $\beta$-sheet structure

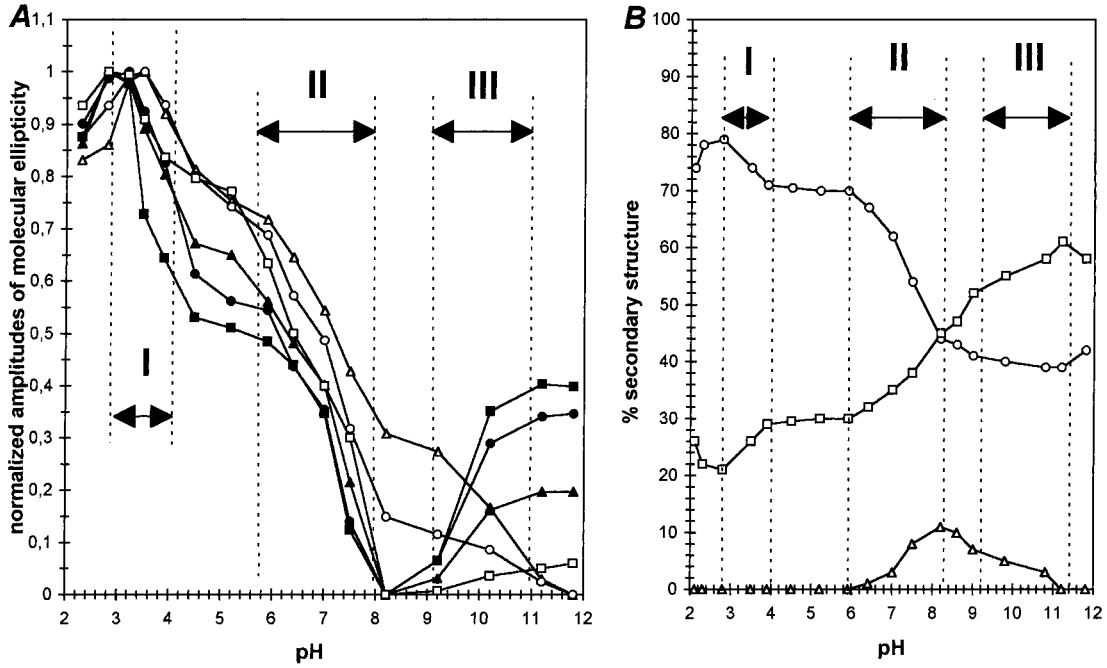


FIGURE 1: Effect of pH on the far-UV CD signals and secondary structure of Ser-32-Grb2-N-SH3 in the absence of salt. (A) Normalized amplitudes of molecular ellipticity (maximum values set to 1 for a given wavelength) as a function of pH at 198 nm (△), 203 nm (○), 208 nm (▲), 215 nm (■), 222 nm (●) or 235 nm (□). All spectra were recorded in phosphate buffer solution (10 mM) at 20 °C. (B) Changes in the secondary structure of Ser-32-Grb2-N-SH3 as a function of pH. Estimation of the secondary structure contents was done by the Provencher procedure: α-helix (△), β-structure (○), and remainder fractions (□). In both figures, the pH domains where transitions I, II, and III take place are delimited by dotted vertical lines.

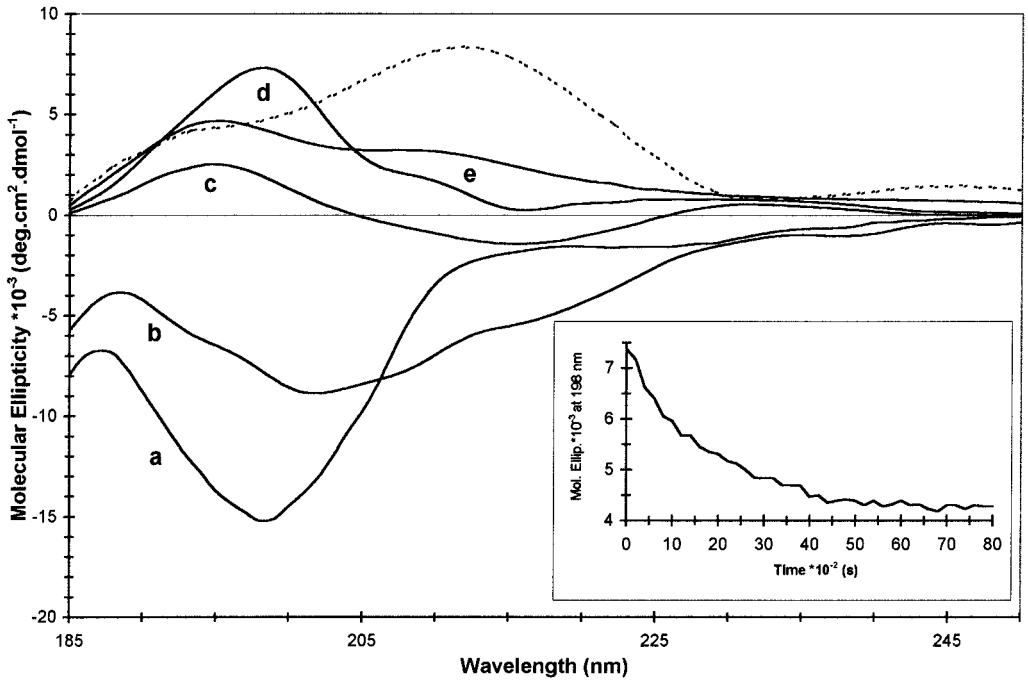


FIGURE 2: Effect of pH on CD profiles of Ser-32-Grb2-N-SH3 in the absence of salt. Far-UV CD spectra (solid lines) are given for the basic conformation at pH = 12 (a), the α/β conformation at pH = 8.2 (b), the all-β conformation at pH = 4.8 (c), and the long-lived kinetic intermediate at pH = 3.2, immediately after HCl addition (d) or after 2 h (e). The difference between spectra e and c is drawn as a dotted line. (Inset) Time dependence of the CD signal at 198 nm at pH = 3.2 (dead time = 30 s).

(*16*). This is substantiated by the estimated secondary structure content, which reveals that this conformation predominantly contains β-structure (70% ± 2%, comprising approximately 45% β-sheet and 25% β-turns) and only 30% ± 2% unordered structure, with no α-helix content being detected. Moreover, a positive CD band is observed at 230 nm (Figure 3A). On account of its position and its positive intensity, this band can be attributed to nonlocal aromatic side-chain interactions, involving spatially close tyrosine residues of the protein (*17*). As such a band results from the local rigidity of the environment, its intensity may be an indicator of the compactness of the protein domain containing these aromatic residues. Generally, such an aromatic contribution to CD profiles leads to an underestimation of helical content (*18*). However, when the maximum intensity of this type of band is low (<2000 deg·cm$^2$·dmol$^{-1}$), the estimation

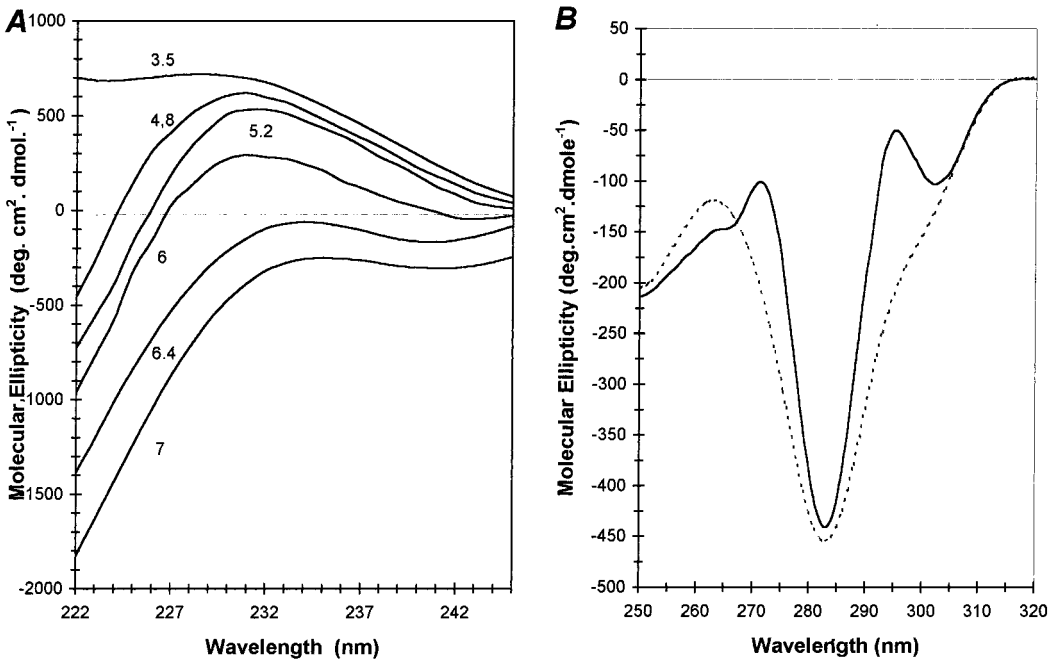


FIGURE 3: Aromatic signals in the CD spectra of Ser-32-Grb2-N-SH3 in the absence of salt. (A) Truncated far-UV CD profiles in the vicinity of 230 nm. The pH values are indicated near the curves. (B) Near-UV CD spectra of the α/*β* conformation at pH = 8.2 (···) and all-*β* conformation at pH = 4.8 (—). Molecular ellipticity is per aromatic residue.

of helical content is weakly affected. This is the case here for the Ser-32-Grb2-N-SH3 domain in the pH range 4−6 and supports the absence of significant helical content. Noticeably, the intensity of the aromatic band is even less at higher pH and may thus not affect the secondary structure evaluation. Taken together, the CD data suggest that the dominant conformation at pH 4−6 corresponds to the native all-*β* conformation; a feature that is further confirmed below.

Moreover, the all-*β* conformation appears to be in equilibrium with a second distinct conformation at more basic pH. The latter is predominant at pH 8−9, as revealed by a plateau in the curves describing the pH dependence of the CD signals (Figure 1A). The CD profile obtained in this pH domain is mainly composed of a large negative peak at 198 nm with two shoulders at 208 and 222 nm (Figure 2) indicating the presence of an α-helical region. This was confirmed by estimation of the secondary structure, which indicates a low amount of α-helix motif. The α-helix content is maximal at pH = 8.2 (10% ± 1%) while the *β*-structure remains the predominant ordered structure (42% ± 2%, comprising approximately 27% *β*-sheet and 15% *β*-turn). It is worth noting that the limited number of residues (five or six) in the helical protein fraction suggests the existence of one or two short helical motifs in the α/*β* conformation, rather than a well-defined α-helix. In contrast to the all-*β* conformation, no broad aromatic band at 230 nm was detected in the α/*β* conformation (Figure 3A), indicating the absence of tertiary aromatic contacts. In this regard, the near-UV spectra of the α/*β* and the all-*β* conformations are also slightly different (Figure 3B). While both of them display a similar prominent negative band at 284 nm, likely related to the Trp-36 residue, the spectrum of the all-*β* conformation is characterized by two small positive peaks emerging at 273 and 295 nm. This suggests some changes in the environment of several tyrosine residues.

Another transition (transition I in Figure 1) occurs when pH is lowered below the values where the all-*β* conformation predominates (pH < 4.8). Initially, transition I is associated with a rapid increase of the main positive band in the short-wavelength domain (Figure 2). In a second phase, the intensity of this band slowly decreases with time (Figure 2, inset). This decrease is accompanied by an overall modification of the CD spectrum that needs about 80 min for stabilization. At pH = 3.2, where this time-dependent phenomenon is most obvious, the CD spectrum observed in the initial phase (Figure 2) is likely related to a long-lived transitional intermediate. In agreement with the slight red shift (3−5 nm) of the positive maximum intensity as compared to the all-*β* CD spectrum, this transient intermediate probably contains *β*-sheets twisted from an ideal planar arrangement (*19*) and/or wrong turns (*20*). Compared to the all-*β* conformation, a distortion of the regular *β*-pleated structure probably occurs in this intermediate conformation.

After stabilization, the transient broad positive band at 200 nm is replaced by a mixture of two less intense peaks at 195 and 210 nm. This indicates that the transient intermediate converts to a mixture of all-*β* conformation and a protein form that probably contains a substantial amount of irregular *β*-turn-like motifs. Interestingly, NMR data obtained in similar conditions (pH = 3, in the absence of salt) (*9*) reveal the existence of a slow equilibrium between the native conformation of the Ser-32-Grb2-N-SH3 domain and a largely but not completely unfolded form. Therefore, the CD bands at 195 and 210 nm may reasonably be attributed to the native and the partially unfolded form, respectively. Accordingly, the all-*β* conformation observed by CD spectroscopy can be considered to be the native conformation of the SH3 domain, which has been earlier elucidated by NMR spectroscopy (*9*−*11*). An approximation of the shape of the CD spectrum of the partially unfolded form is given by the difference between the spectrum recorded at pH = 3.2, after stabilization, and that recorded at pH = 4.8 (Figure 2). Note that, as a function of pH, transition I is almost completely

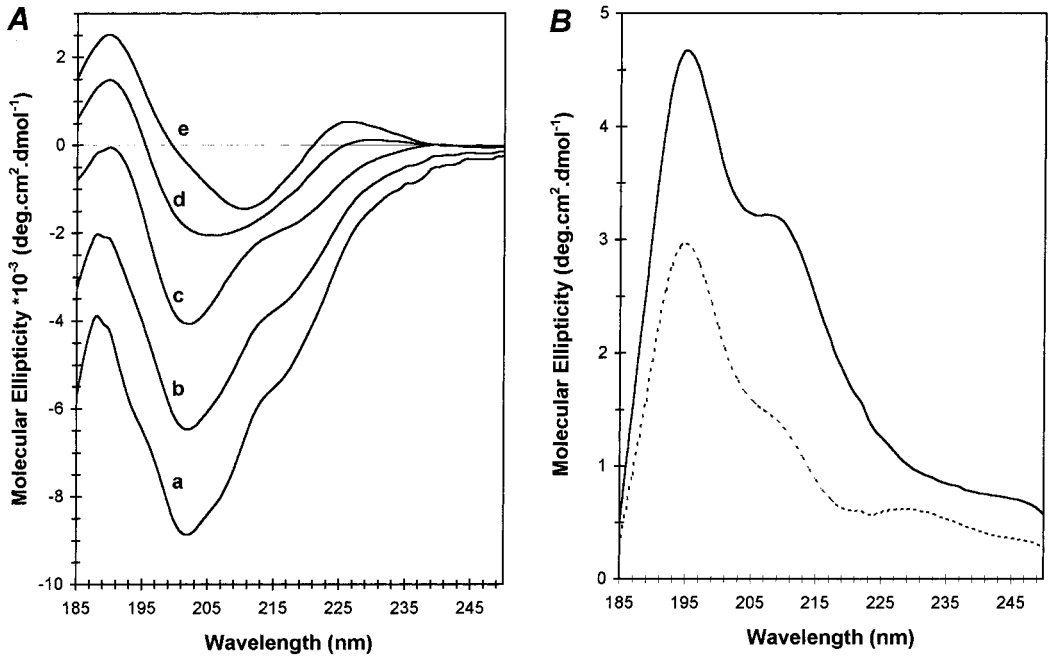


FIGURE 4: Salt effect on the CD spectra of Ser-32-Grb2-N-SH3. (A) Salt-induced changes in the far-UV CD spectra of Ser-32-Grb2-N-SH3 at pH = 8.2. The NaCl concentrations are 0 mM (a), 30 mM (b), 80 mM (c), 120 mM (d), and 180 mM (e), respectively. (B) Salt-induced changes in the far-UV CD spectra at pH = 3.2. The NaCl concentrations are 0 (—) and 120 mM (•••), respectively.

reversible at short times, while only a poor reversibility is observed after stabilization of the CD signals at long times.

A third transition (transition III in Figure 2) is observed for pH values between 9 and 11. This transition is associated with a modification of the CD spectrum of the α/*β* conformation, that irreversibly results in the basic profile identified at pH = 12 (Figure 2). Given that the protein domain is not stongly hydrolyzed at this pH (data not shown), this spectrum may represent a predominant basic conformation, devoid of α-helix content and with substantial *β*-structure content (40% ± 2%) being retained.

*Salt Effect*. As the ionic strength plays an important biological role in the stabilization of protein structure, the effects of salt addition on the conformations reported above were investigated. For the α/*β* conformation, increasing the ionic strength by salt addition at pH = 8.2 results in large changes in the far-UV CD spectra (Figure 4A), in relation with an increase of *β*-structure at the expense of both α-helix content and random fraction. This may well correspond to a shift in the equilibrium between the α/*β* and the all-*β* conformations toward the latter conformation. Indeed, at 180 mM NaCl, the CD profile is very similar to that of the all-*β* conformation (compare Figure 4A, curve e, with Figure 2, curve c), indicating a complete shift of the equilibrium. Interestingly, the more substantial the initial contribution of the all-*β* conformation, the less salt is needed to completely shift the equilibrium. Similarly, the addition of salt at pH = 3.2 decreases the band at 210 nm and increases the ratio of the signals at 195 and 210 nm (Figure 4B), suggesting a shift in the equilibrium between the native all-*β* conformation and the partially unfolded form in favor of the former. This observation matches NMR data (*9*) and points out that an increase in the ionic strength favors the formation of the native all-*β* conformation, at all pH values (with the exception of of pH > 11, where no significant changes in the CD profiles are detected, upon salt addition).

*Temperature Effect*. Temperature-induced changes in CD spectra are strongly pH-dependent, suggesting that the observed thermal transitions depend on the nature of the SH3 domain conformation. Under conditions where the all-*β* conformation is predominant (pH = 4.8, no salt), significant changes are seen in the far-UV CD spectra upon heating (Figure 5A), with the secondary structure of the all-*β* conformation being largely affected. Even though the decrease of the total *β*-structure apparently follows a single-step transition from 25 to 80 °C, two steps are actually involved in the overall transition, as shown by the individual fractional changes in helical and random coil fractions (Figure 5B). The first step can be distinguished by the sigmoid-shaped curve relating to the increase in the random fraction. The midpoint temperature $T_{M1}$ at 35 ± 2 °C and the low corresponding van't Hoff enthalpy (27 ± 3 kcal·mol$^{-1}$), indicate a weak thermal stability of the native all-*β* conformation. Interestingly, together with a limited increase in the random fraction, this first step is essentially related to a depletion of the *β*-turn content, probably corresponding to a loss of protein compactness (*21*). The sigmoid-shaped curve related to α-helix formation accounts for the second step (45−80 °C), with a midpoint temperature $T_{M2}$ at 56 ± 2 °C and a corresponding van't Hoff enthalpy of 53 ± 2 kcal·mol$^{-1}$. In this second step, the *β*-structure decay mainly concerns *β*-sheet content, which drops from 45% to 25%, for the most part in favor of α-helix structure. The presence of two consecutive steps is corroborated by the profile of the decrease of the CD band at 230 nm, as a function of temperature (Figure 5A, inset). A smooth shoulder emerges between 35 and 45 °C, indicating an intermediate state in the overall thermal transition. In these conditions, only a disruption of tertiary contacts seems to be involved and it can be suggested that the thermal intermediate formed at 40 °C is a molten globule-like form, as is frequently observed in thermal transitions of globular

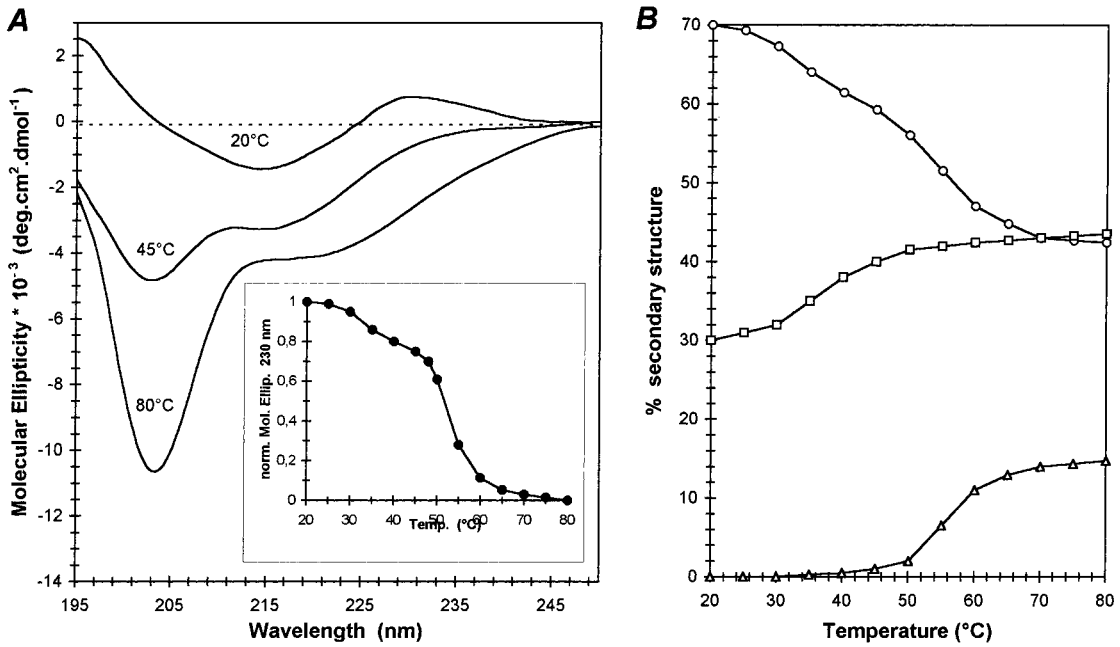


FIGURE 5: Heating of Ser-32-Grb2-N-SH3 at pH = 4.8 in the absence of salt. (A) Temperature effect on the far-UV CD spectrum of the native all-$\beta$ conformation. (Inset) Extent of the aromatic tertiary interaction. Reduced molecular ellipticities at 230 nm were calculated by: $\Theta_{230} - (\Theta_{240} - \Theta_{220})/2$ and normalized to 1. (B) Temperature effect on the main components of the secondary structure: $\alpha$-helix ($\triangle$), $\beta$-structure ($\bigcirc$), and remainder fractions ($\square$), as estimated by the Provencher procedure.

proteins (*22*). Interestingly, the structure of this expanded nonnative conformation does not change when the temperature is lowered to 20 °C, suggesting the irreversibility of the first step in the thermal transition. In contrast, the second step between 45 and 75 °C is fully reversible and involves partial conversion of the $\beta$-structure to helical motifs, leading to an $\alpha/\beta$ conformation resembling that observed at ambient temperature at pH = 8.2. In addition, it is worth noting that, upon salt addition (180 mM NaCl) at ambient temperature, the globulelike form resulting from the heating/cooling cycle at pH = 4.8 converts to the native all-$\beta$ conformation.

Furthermore, heating of the SH3 domain at pH = 3.2 in the absence of salt, where the native all-$\beta$ conformation is in equilibrium with a partially unfolded form, was also done (data not shown). At 70 °C, the global $\beta$-content decreases, mostly in favor of the random fraction. However, CD signals indicating a low helical content are also observed. This may result from the formation of a largely unfolded form containing some helical motifs. However, helical CD signals are no longer present when the temperature is lowered to 20 °C, and the ratio of the signals at 195 and 210 nm is decreased. This suggests a conversion of the helical motifs formed at high temperature into $\beta$-turn-like motifs at ambient temperature.

On the other hand, regarding the $\alpha/\beta$ conformation that prevails at pH = 8.2 in the absence of salt, an apparent single-step transition is observed when the temperature is increased to 70 °C (data not shown). The global $\beta$-content decreases from 53% to 16%, mostly in favor of random fractions (from 38% to 68%), while the $\alpha$-helical content is moderately increased (from 10% to 17%). All transitions associated with the change in secondary structure contents have a similar melting temperature of 42 ± 2 °C, the corresponding $\Delta H(T_M)$ being 34 ± 3 kcal·mol$^{-1}$. The $\alpha/\beta$ conformation appears therefore to be slightly more temperature-resistant than the all-$\beta$ conformation, particularly as far as tertiary structure is concerned. The CD spectra obtained at high temperature may be accounted for by an equilibrium between the $\alpha/\beta$ conformation and a partially unfolded form containing helical motifs as the only ordered fraction. Upon cooling to ambient temperature, the amount of the $\alpha/\beta$ conformation is slightly decreased, but a low amount of a partially unfolded form containing $\beta$-turn-like motifs is apparently formed. This partially unfolded form, containing helical motifs at high temperature and $\beta$-turn-like motifs at ambient temperature, may be similar to that observed at acidic pH. Finally, the CD profile at pH = 12 did not vary significantly with increasing temperature.

*Chemical Unfolding*. Guanidine hydrochloride (GdnHCl) and urea were used as chaotropic agents to investigate the unfolding of Ser-32-Grb2-N-SH3. Upon addition of GdnHCl, large changes in far-UV CD spectra are observed at pH = 4.8 in the absence of salt, where the all-$\beta$ conformation predominates (Figure 6A). Due to the absorption properties of GdnHCl, the spectra are truncated at 200 or 205 nm, depending on the denaturant concentration. The denaturation follows a two-step process. Depending on wavelength, the CD signals showed either a maximum or a shoulder at 0.5 M GdnHCl (Figure 6B). The CD profile at 0.5 M GdnHCl (Figure 6A, curve b) resembles the spectrum observed at pH = 3.2 in the absence of salt (Figure 2, curve e). As this acid spectroscopic state may correspond to a mixture of the all-$\beta$ conformation and a partially unfolded form of the SH3 domain, we suggest that this last form could also be a protein intermediate involved in the unfolding pathway. At denaturant concentrations above 2 M, only a completely unfolded form that results from the second step of the denaturation is observed. These data were interpreted by use of a three-state reaction scheme:

$$N \overset{K_1}{\rightleftharpoons} I \overset{K_2}{\rightleftharpoons} U \qquad (3)$$

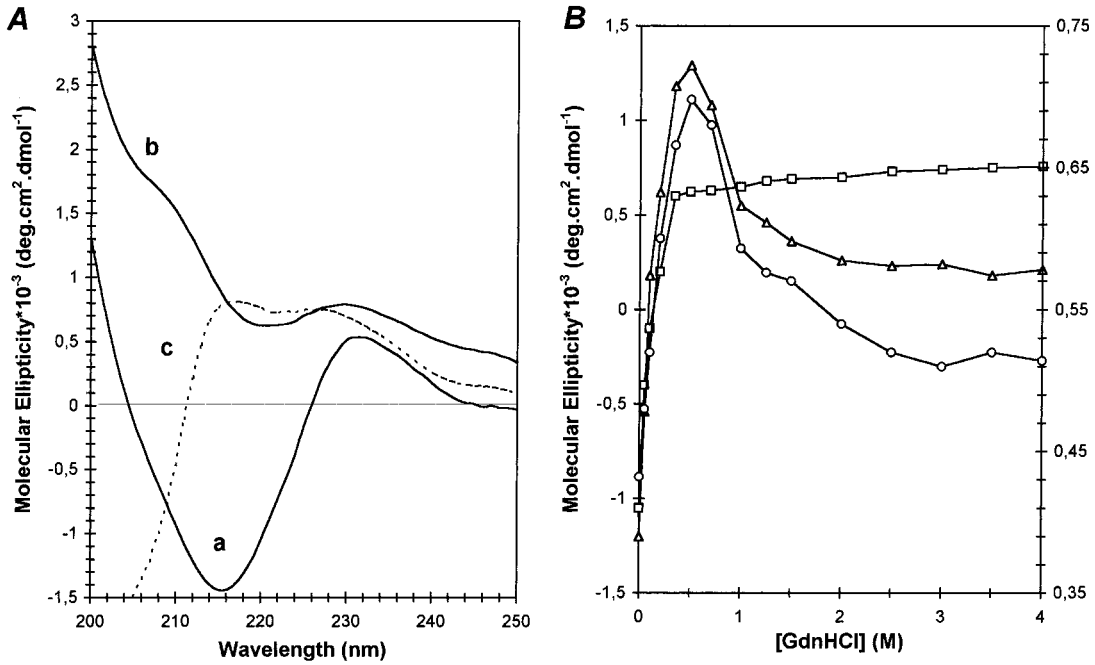


FIGURE 6: Denaturation of Ser-32-Grb2-N-SH3 with GdnHCl at pH = 4.8 in the absence of salt. (A) Far-UV CD spectra with GdnHCl concentrations of 0 mM (a), 500 mM (b), and 4 M (c). (B) Plots of CD signal intensities at 212 nm (△), 220 nm (□), and 235 nm (○). The 212 and 220 nm intensities are scaled by the left ordinate axis, while the 235 nm intensities are scaled by the right ordinate axis.

Table 1: Thermodynamic Parameters Describing the Unfolding of Ser-32-Grb2-N−Sh3 at Critical pH Values with GdnHCl or Urea as Denaturing Agents[a]

| | $\Delta G_{0,1}^{H_2O}$ (kcal·mol$^{-1}$) | $\Delta G_{0,2}^{H_2O}$ (kcal·mol$^{-1}$) | $m_1$ (kcal·mol$^{-1}$·M$^{-1}$) | $m_2$ (kcal·mol$^{-1}$·M$^{-1}$) | $C_{M,1}$ (M) | $C_{M,2}$ (M) |
|---|---|---|---|---|---|---|
| | | | GdnHCl | | | |
| pH 4.8 | 1.7 ± 0.1 | 2.5 ± 0.1 | 14 ± 2 | 3.1 ± 0.1 | 0.25 ± 0.05 | 0.9 ± 0.1 |
| pH 8.2 | 2.3 ± 0.1 | | 1.8 ± 0.2 | | 0.5 ± 0.1 | |
| pH 12 | 1.3 ± 0.1 | | 0.9 ± 0.1 | | 1.4 ± 0.1 | |
| | | | Urea | | | |
| pH 4.8 | 1.5 ± 0.05 | 2 ± 0.1 | 11 ± 1 | 1 ± 0.5 | 0.25 ± 0.05 | 2 ± 0.1 |
| pH 8.2 | 2.1 ± 0.1 | | 1.6 ± 0.1 | | 1.4 ± 0.1 | |

[a] All experiments were performed in phosphate buffer (10 mM), at 20 °C, in the absence of salt. Subscripts 1 and 2 refer to the first and second transition, respectively, for the three-state model applied.

where N is the native conformation, with I and U being the intermediate form and the completely unfolded form of the SH3 domain, respectively. $K_1$ and $K_2$ are the equilibrium constants for the transitions. The CD signal at 220 nm, $Y$, can be expressed as

$$Y = \frac{Y_N + K_1 Y_I + K_1 K_2 Y_U}{1 + K_1 + K_1 K_2} \quad (4)$$

where $Y_N$, $Y_I$, and $Y_U$ are the CD signals assigned to N, I, and U, respectively. Assuming the linear extrapolation model (LEM) (*23*), the constants $K_1$ and $K_2$ can be written as

$$K_1 = \exp\{(m_1[D] - \Delta G_{0,1}^{H_2O})/RT\} \quad (5)$$

$$K_2 = \exp\{(m_2[D] - \Delta G_{0,2}^{H_2O})/RT\} \quad (6)$$

where [D] is the GdnHCl concentration and $\Delta G_{0,1}^{H_2O}$ and $\Delta G_{0,2}^{H_2O}$ are the free energy changes associated with the transitions, in the absence of GdnHCl. The $m_1$ and $m_2$ values are generally correlated with the change in hydrophobic surface exposed to solvent *(24)* and may also be considered as cooperativity indexes (*25*). Substitution of eqs 5 and 6 in eq 4 provides the equation with which the experimental data were fitted. Accordingly, a low free energy gap was estimated to separate the all-$\beta$ conformation and the intermediate form (Table 1). The CD profile of this intermediate was evaluated from the CD spectrum at 0.5 M GdnHCl by subtracting the spectral contributions of both the all-$\beta$ conformation and the unfolded form. It turns out that the CD profile of the intermediate form resembles the estimated profile of the partially unfolded form at pH = 3.2 (Figure 2). These findings suggest that the partially unfolded form of the SH3 domain is in the unfolding pathway of the native all-$\beta$ conformation, when GdnHCl is used as a denaturant.

At pH = 4.8, in the absence of salt, the urea-induced changes in the CD spectra were also studied (Figure 7). As for GdnHCl, a two-step process was observed. However, while the CD signals increase for low GdnHCl concentrations, they decrease with urea. A marked minimum intensity around 0.5 M urea was seen at 220 nm (Figure 7, inset). As observed with GdnHCl, this can reasonably be assumed to correspond to the formation of an intermediate form in the unfolding pathway. To evaluate the profile of this intermediate form, the CD spectrum recorded at 0.5 M urea was resolved, as above for GdnHCl. The obtained profile resembles that of the $\alpha/\beta$ conformation. This suggests that the protein intermediate, whose contribution is maximal at

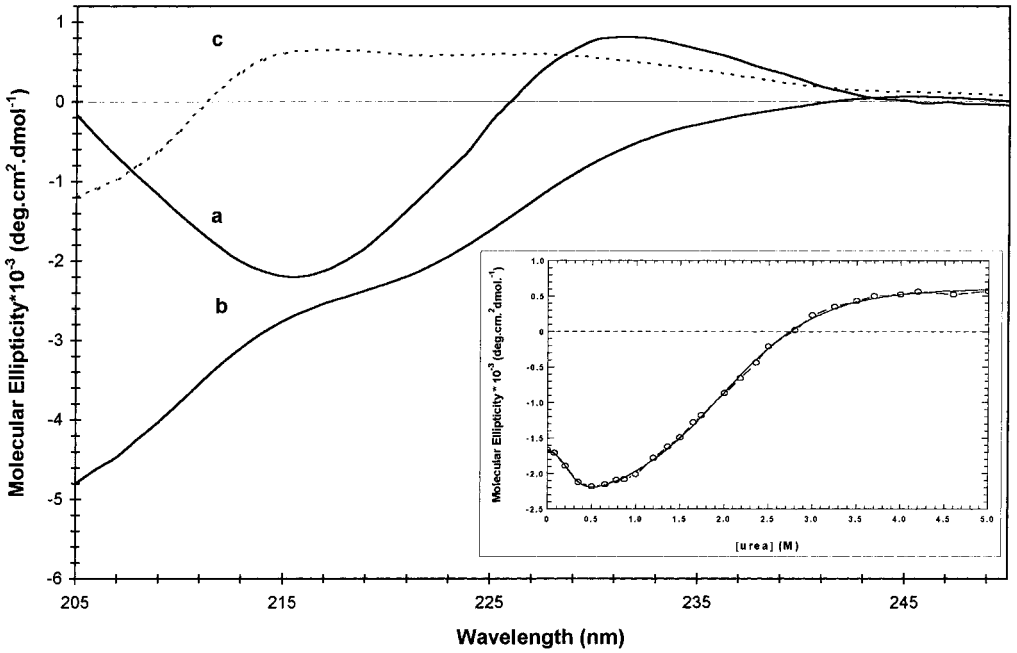


FIGURE 7: Denaturation of Ser-32-Grb2-N-SH3 with urea at pH = 4.8 in the absence of salt. Far-UV CD spectra with urea concentrations of 0 m M (a), 500 mM (b), and 5 M (c) are shown. (Inset) Fit of the CD signal intensity at 220 nm (○) to a three-state unfolding model (—).

0.5 M urea, could be the α/*β* conformation, being thus separated from the all-*β* conformation by a low free energy gap (Table 1). If true, the α/*β* conformation probably differs from the all-*β* conformation by a less condensed protein exterior, consistent with the high *m* value associated with the first transition step.

Accordingly, the unfolding pathway from the all-*β* conformation depends on the denaturant. The protein intermediates involved in the two denaturation processes have different secondary structures but similar thermodynamic properties. Although this is unusual, such subtle differences in the denaturing effects of GdnHCl and urea have been previously reported (*26*) and were suggested to result mainly from the specific electrostatic interactions between the protein and the denaturant.

Denaturation studies at pH = 8.2 in the absence of salt, where the α/*β* conformation is predominant, were also done with GdnHCl and urea (Table 1). In both cases, a single-step process was observed. Noticeably, the free energy gap associated with the unfolding of the α/*β* conformation does not significantly depend on the nature of the denaturant. Moreover, this free energy gap is close to that estimated for the second step of the denaturation of the native all-*β* conformation. This is in line with the involvement of the α/*β* conformation in the unfolding process of the native all-*β* conformation when using urea. Finally, a two-state model also applies to the denaturing process induced by GdnHCl at pH = 12. Provided that in these conditions a distinct basic *β*-form is involved, its Gibbs energy is close to that of the completely unfolded form, with a similar extensive solvent exposure of its surface.

*Effect of Mutation*. The double mutant Y7V/C32S, in which the Tyr-7 residue of Ser-32-Grb2-N-SH3 (C32S) was replaced by a valine, was studied. This point mutation was expected to be crucial for the functionality of the SH3 domain since a similar mutation in the SH3 domain from Sem-5 reduces the binding to a proline-rich peptide, without drastic change in the protein conformation (*27*, *28*). At pH = 8.2 in the absence of salt, the spectrum of Y7V/C32S significantly differs from that of C32S, exhibiting a more intense negative band at 200 nm as a main feature (Figure 8A). This suggests that an α/*β* conformation similar to that of C32S is accompanied by another form. Upon this assumption, a CD profile is obtained by subtracting the spectrum of the α/*β* conformation of C32S from the experimental spectrum at pH = 8.2 (Figure 8B), indicating that this exchanging form is devoid of α-helix and includes some *β*-turns.

To further compare Y7V/C32S and C32S, the effects of a pH decrease from 8.2 to 4.8 on both SH3 domains were also examined (Figure 8A). In contrast to C32S, the CD signals for Y7V/C32S at pH = 4.8 are time-dependent, needing about 1 h before reaching stability. The intense positive band initially detected at 198 nm decreases slowly to give rise to two bands centered at 195 and 210 nm. Assuming a contribution of an ordered all-*β* conformation as for C32S, the shape of the CD profile of the remaining protein form after stabilization can be estimated (Figure 8B). Being entirely positive and exhibiting a main large broad band centered around 215 nm, it resembles the spectrum estimated for the partially unfolded form of C32S at pH = 3.2 (Figure 2). Moreover, no shoulder in the CD signals versus pH was observed for Y7V/C32S, in the pH 4−6 range (data not shown). This suggests that no distinct protein form is predominant in this pH domain, in contrast to C32S. Instead, there is probably a mixture of the native all-*β* conformation and a partially unfolded form, with the contribution of the latter increasing at acid pH. Thus, the Y7V/C32S and the C32S mutants have probably similar native all-*β* and α/*β* conformations, but they differ by the distribution of these conformations. In the near-UV domain (Figure 8C), the CD spectrum of Y7V/C32S at pH = 4.8 differs from that of C32S by the absence of small peaks at 270 and 293 nm, indicating that their formation depends on the Tyr-7 residue.

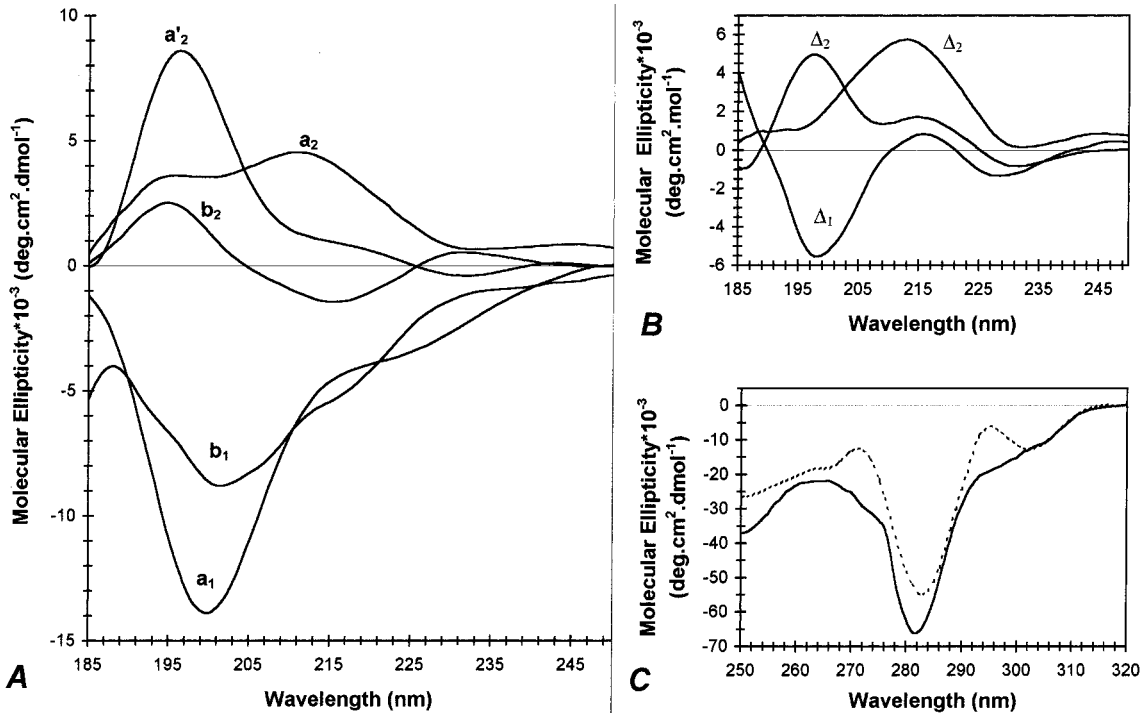


FIGURE 8: Mutation effect on CD spectra. (A) Far-UV CD spectra of the double mutant Y7V/C32S ($a_1$, $a'_2$, and $a_2$) and Ser-32-Grb2-N-SH3 (C32S) ($b_1$ and $b_2$) in the absence of salt. Spectra $a_1$ and $b_1$ were recorded at pH = 8.2, while spectra $a'_2$, $a_2$, and $b_2$ were recorded at pH 4.8. The spectrum of Y7V/C32S was recorded before ($a'_2$) and after 1 h of stabilization ($a_2$). (B) Difference spectra between the Y7V/C32S and C32S spectra at pH = 8.2 ($\triangle_1 = a_1 - b_1$) and at pH = 4.8 before ($\triangle_2' = a'_2 - b_2$), and after 1 h of stabilization ($\triangle_2 = a_2 - b_2$). (C) Near-UV spectra of Y7V/C32S (—) and of C32S (···) at pH 4.8 in the absence of salt.

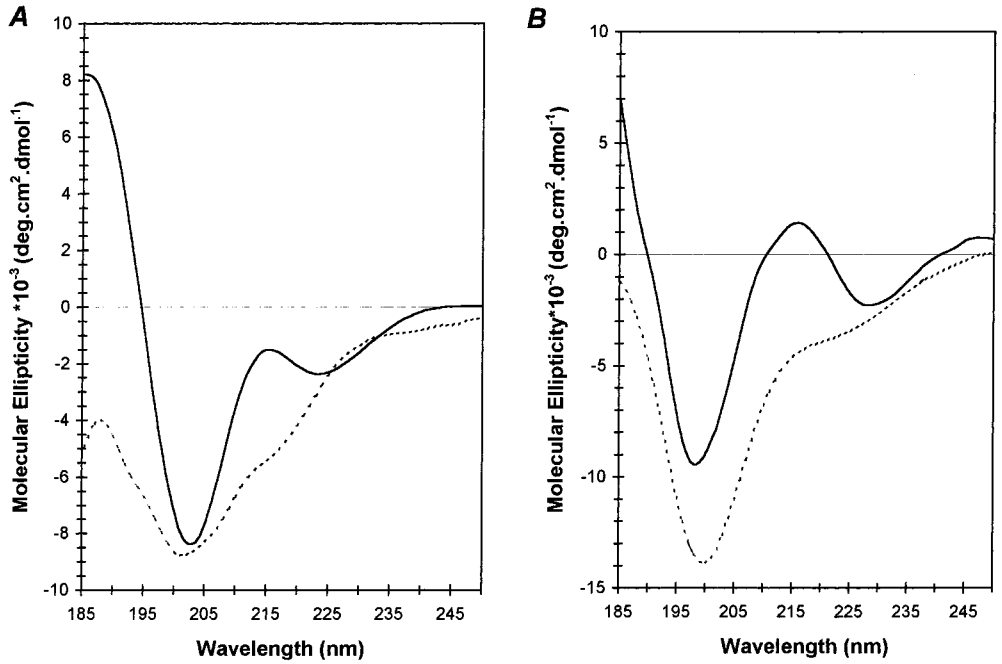


FIGURE 9: Effect of environment hydrophobicity on the CD spectra of Ser-32-Grb2-N-SH3 and Y7V/C32S in the absence of salt. Far-UV CD spectra of C32S (A) and Y7V/C32S (B) at pH = 8.2, in the absence (···), and in the presence (—) of SDS in submicellar concentration (6 mM), are shown.

*Effect of Environment Hydrophobicity*. SDS in submicellar concentrations was progressively added to the buffer in order to increase the hydrophobicity of the environment. In conditions where the $\alpha/\beta$ conformation is predominant (pH = 8.2 in the absence of salt), a two-state transition is observed for SDS concentrations between 2 and 6 mM. The far-UV CD spectrum of the resulting protein form is consistent with an all-$\beta$ form containing $\beta$-turn-like motifs, as seen by the band centered at 215 nm (Figure 9A). This suggests that the $\alpha$-helical region of the $\alpha/\beta$ conformation converts to $\beta$-turn-like motifs. As a result, the resulting protein may correspond to a nonnative all-$\beta$ conformation, differing from the native one by an increased $\beta$-turn content and by the absence of tertiary aromatic contacts, as suggested by the absence of the aromatic band at 230 nm. Interestingly, upon salt addition, this nonnative conformation was found

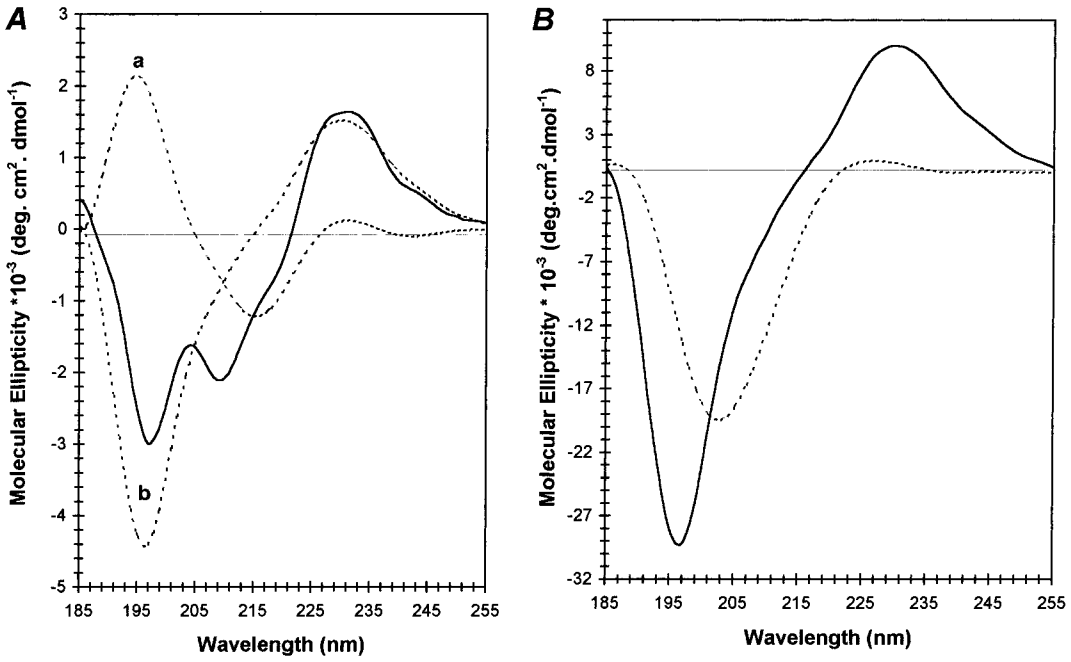


FIGURE 10: Binding of Ser-32-Grb2-N-SH3 to the proline-rich VPPPVPPRRR decapeptide at pH = 7, $T$ = 20 °C, in the absence of salt. (A) Resolution of the spectrum of the SH3−peptide complex (—). The spectral contributions of the bound SH3 domain (a) and the bound decapeptide (b) were deduced by assuming that the conformation of the SH3 domain in the complex is the native all-$\beta$ one. (B) Comparison of the far-UV CD spectrum of the free proline-rich decapeptide (···) with that evaluated for the bound peptide in the SH3-peptide complex (—).

to convert to the native one. It is worth noting that the addition of submicellar SDS to the mutant Y7V/C32S at pH = 8.2 similarly increases the contribution of the nonnative all-$\beta$ conformation exchanging with the $\alpha/\beta$ conformation (Figure 9B).

*Binding with a Proline-rich Peptide.* A very attractive point in the study of SH3 domains is their ligand specificity. Here, the proline-rich VPPPVPPRRR decapeptide derived from h-Sos was chosen because of its good affinity for the N-terminal SH3 domain of Grb2 (*9*−*11*). The binding experiments were performed at neutral pH. At this pH, the far-UV CD spectrum of the free form of the proline-rich decapeptide is essentially characterized by a negative peak at 202 nm with a mid-intensity about $2 \times 10^4$ deg·cm$^2$·dmol$^{-1}$, consistent with a poorly ordered polyproline helix (*29*, *30*). The far-UV CD spectrum of the complex was obtained from the measured spectrum by subtracting the spectral contribution of the free SH3 domain and that of the peptide excess (Figure 10A). Since NMR data have shown that only the native all-$\beta$ conformation binds to the decapeptide (*9*), the shape of the far-UV CD profile of the bound decapeptide can be further obtained by subtracting the spectral contribution of the all-$\beta$ conformation from the spectrum of the complex (Figure 10A). The individual spectrum exhibits two distinct changes, compared to the free peptide (Figure 10B). The first concerns the noticeable intensity increase and the slight blue-shift (202 → 196 nm) of the negative peak. This can be associated with the folding of the decapeptide since similar changes were observed in conditions favoring the formation of the polyproline helix, as, for example, in the presence of trifluoroethanol (TFE) and/or upon heating. The second change relates to the formation of a broad positive band centered at 228 nm, which will be discussed below.

Significant changes in near-UV CD spectra were also observed, upon addition of increasing decapeptide concentrations (Figure 11). As the decapeptide does not exhibit a CD signal in this region, these spectra can be entirely attributed to the aromatic residues in the SH3 domain. The spectral changes mainly concern the emergence of a weak band at 273 nm and an increasingly intense peak at 295 nm. The positions of these peaks and the ratio of their maximum intensities are both consistent with an exciton interaction between electronic transitions in neighboring aromatic side chains. Exciton interaction arises from the coupling of absorption dipoles of identical chromophores, which would have the same energy if they do not interact (*31*, *32*). As a result, a splitting of the common CD band is observed, in which the extent of the separation of the two bands depends on the amplitude of dipole interactions and the ratio of their maximum intensities on the spatial geometry of both electronic dipole transition moments. Owing to the absence of these bands in the near-UV spectrum of the mutant Y7V/C32S (Figure 8C) where Tyr-7 is lacking, on one hand, and to the close location of Tyr-7 and Tyr-52 in the native all-$\beta$ conformation (9), on the other hand, these Tyr residues likely participate in this exciton formation. Considering that at a ratio of decapeptide to protein concentration > 8 the binding reaction is nearly complete, the spectral contribution of this exciton to the near-UV CD spectrum of the bound SH3 domain can be estimated (Figure 11, inset). The main spectral feature differentiating the exciton profile before and after binding is a large increase (from 1.2 to 20) in the ratio of the maximum intensities of the two positive peaks. This likely results from a substantial change in the relative orientation of the phenolic rings of Tyr-7 and Tyr-52, reflecting a binding-induced modified geometry of their spatial arrangement. Interestingly, the monitoring of the CD signal at 295 nm proves to be suitable for evaluating the SH3 domain affinity for the proline-rich peptide, giving an

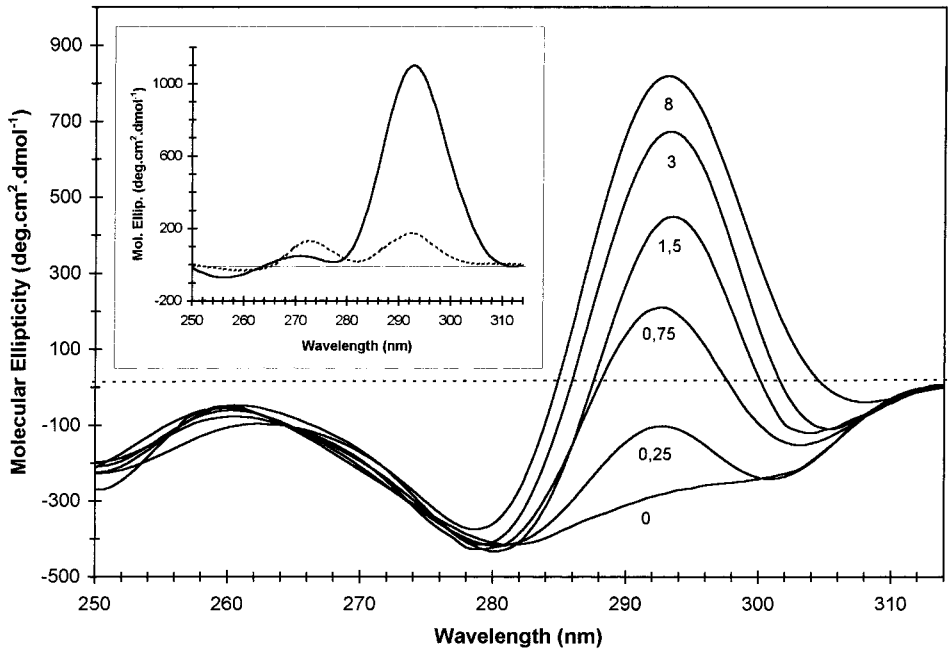


FIGURE 11: Near-UV CD spectra of Ser-32-Grb2-N-SH3 upon binding with the proline-rich VPPPVPPRRR decapeptide. The peptide to SH3 domain concentration ratios are reported below the curves. Spectra were recorded at pH = 7, $T$ = 20 °C, in the absence of salt. (Inset) Spectral contributions of exciton before (···) and after (—) binding to the decapeptide were evaluated by use of, as a baseline, the near-UV spectrum of the α/$\beta$ conformation, which is devoid of the contribution of the exciton. Molecular ellipticity is per aromatic residue.

apparent affinity (4.6 $\mu$M) very similar to that found from fluorometric titration (4 $\mu$M) (*33*).

## DISCUSSION

*CD Structural Features of the Distinct Conformations Adopted by the Isolated SH3 Domain*. One of the main features of the present study is the evidence of a pH region around 4.8, where the CD spectrum and, thus, the secondary structure of Ser-32-Grb2-N-SH3 domain are invariant in the absence of salt. The CD spectrum in this pH region is similar to that at pH 6.0 in the presence of 100 mM salt. Since NMR data have shown that in the latter conditions only the native all-$\beta$ conformation is present, we suggest that this conformation may also be predominant at pH 4−6 in the absence of salt. This conclusion is at variance with the equilibrium between this native conformation and an unfolded form that has been observed by NMR for either the wild-type SH3-domain at pH 6.5 (*34*) or the related SH3-domain of drk at pH 6 (*35*−*38*). Accordingly, we suggest that the mutation of Cys32 to Ser in the Grb2-N-SH3 domain may have a stabilizing effect similar to that of D48G substitution in the α-spectrin SH3 domain (*39*) or (T22G, Q23D) replacement in the drk SH3 domain (*38*).

In full keeping with NMR data of this mutant SH3 domain (*9*) or the corresponding wild-type SH3 domain (*10*, *11*), the CD structural features that characterize the native all-$\beta$ conformation of Ser-32-Grb2-N-SH3 highlight a large $\beta$-sheet content, in a compact all-$\beta$ structure. However, the absence of α-helix content detectable by CD spectroscopy is somewhat surprising, when compared to the conserved one-turn $3_{10}$ helix evidenced by NMR in the C-terminal part of the SH3 domain. The reason is probably that the CD signal of the $3_{10}$ helix, which is similar to that of α-helix (*40*), depends not only on the amount of helical moiety but also on the helix length. Indeed, when ellipticity at 222 nm is used as a specific helix content indicator, experimental values deviate negatively from linearity by a factor equal to $(1 - 2.5/n)$, where $n$ is the number of peptide bonds (*17*). This is not very significant for $n \geq 10$ but for $n = 3$, the CD signal is no more detectable.

It is worth noting that the narrow pH domain where the native form predominates in the absence of salt is very close to the isoelectric point (p$I$ = 5.5). This agrees well with the smeared charge model in which electrostatic repulsion at the protein surface acts to unfold the protein unless it is balanced by strong hydrophobic interactions (*28*, *41*). In this respect, several acidic residues are close to the aromatic residues that form the smooth hydrophobic platform on the surface of the native form (*9*). Accordingly, either by setting the pH value close to the p$I$ value or by increasing the ionic strength, the electrostatic repulsion between these acidic residues may be reduced, a feature that favors the hydrophobic interactions between the aromatic residues.

Interestingly, the formation of the external tertiary contacts appears to be concomitant with the completion of the inner $\beta$-structure. Such nonhierarchical folding, involving a concerted formation of tertiary and secondary structures, has been previously reported for the SH3 domains from Src (*42*) and from α-spectrin (*43*). More generally, this is relevant for small all-$\beta$ proteins, where side-chain interactions could determine the final $\beta$-sheet architecture (*44*). In this respect, the Gibbs energy of stabilization associated with the native form, as measured by chemical unfolding with GdnHCl (4.2 kcal·mol$^{-1}$) or urea (3.5 kcal·mol$^{-1}$), fits fairly well with those reported for the SH3 domains from BTK (2.6 kcal·mol$^{-1}$) (*45*), α-spectrin (3.3 kcal·mol$^{-1}$) (*46*), PI3-kinase (3.38 kcal·mol$^{-1}$) (*47*), Sem-5 (4.1 kcal·mol$^{-1}$) (*28*), and chicken src (4−4.7 kcal·mol$^{-1}$) (*42*). This supports that the N-SH3 domain from Grb2 is thermodynamically unstable, like its nonhuman homologues.

In full keeping with NMR data (*9*, *34*), the CD data at low pH values (≈3) reveal the existence of an equilibrium

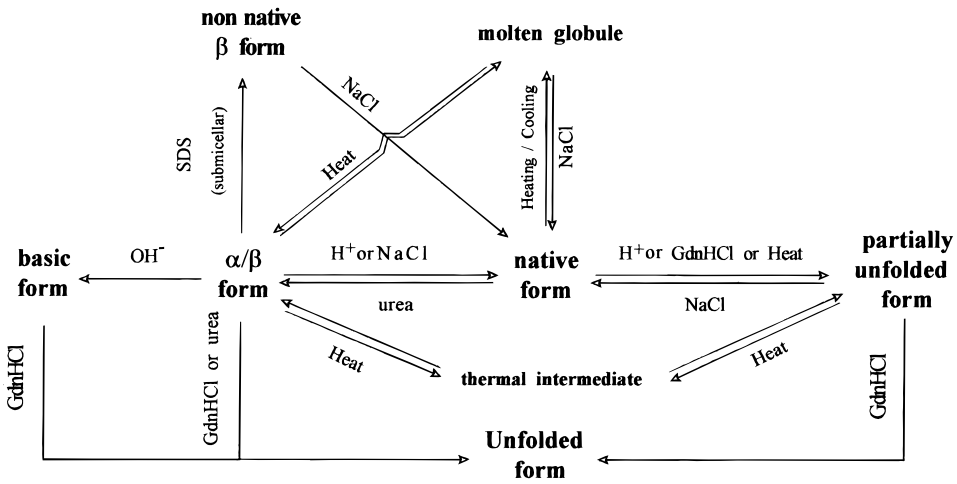


FIGURE 12: Schematic representation of the relationships between the distinct CD conformations observed for Ser-32-Grb2-N-SH3 in the absence of salt. The thermal intermediate is observed at $T = 70$ °C.

between the native conformation and a partially unfolded form in the absence of salt (Figure 12). Moreover, according to the higher acquisition speed of CD as compared to NMR spectra, we additionally show that the partially unfolded form results from the relaxation of a long-lived transitional state containing mistwisted $\beta$-structure. The shape of the far-UV CD profile estimated for the partially unfolded form is unusual, but it may reflect that the only ordered motifs are $\beta$-turn-like, given the broad positive band exhibiting a maximum intensity around 215 nm. The lack of a significant band at 230 nm indicates the absence of tertiary contacts and is a hint about the external looseness of the partially unfolded form. In addition, the chemical unfolding with GdnHCl as a denaturing agent shows that the partially unfolded form is probably involved, as a poorly condensed protein intermediate in the unfolding pathway of the native form. Topological insight of the structural interactions existing within the partially unfolded form was previously provided by NMR data suggesting the existence of sequential NOEs in two protein fragments, located between the residues Asn-35 and Ala-39 and between the residues Lys-44 and Phe-47, respectively (*34*). Such an equilibrium between the native conformation and a partially unfolded form was also evidenced by NMR for the SH3 domains of α-spectrin (*46*) and drk (*35*). For the latter, which shares 72% identity with the Grb2 N-SH3 domain, sequential NOEs have been observed in the peptide segment from Asn-35 to Ile-48 (*36*), within the loosely packed conformation existing under nondenaturing conditions. It was suggested that the residues in this region adopt turnlike structures that preferentially sample the α region of the dihedral conformational space (*37*), thereby having potential helical properties.

At neutral and basic pH, the native conformation is found in equilibrium with an α/$\beta$ conformation. This α/$\beta$ conformation predominates at pH = 8.2 in the absence of salt and is the only conformation that contains stable helical motifs in nondenaturing conditions. Globally, the interconversion between the native and α/$\beta$ forms probably depends on $\beta$-sheet ⇔ α-helix switching of short peptide fragments involving only 5−6 residues. This switching is associated with and possibly triggered by a change in the compactness of the external structure. In contrast to the native and the partially unfolded forms, no NMR data are available for the α/$\beta$ form. Therefore, the localization of the secondary structural elements cannot be straightforwardly assessed. As for the drk N-SH3 domain (*38*), the partially unfolded state of the Grb2 N-SH3 domain is probably composed of an ensemble of interconverting conformers sharing a common topology in their nonnative secondary structure. It can therefore be speculated that both α/$\beta$ and partially unfolded forms, which have similar Gibbs energy and share the ability to exist under nondenaturing conditions, belong to such a conformational ensemble. In this respect, the helical motifs in the α/$\beta$ form may be formed from the potential helical regions defined by the sequential NOEs in the partially unfolded form (*34*). This is further supported by the interconversion at high temperature of the α/$\beta$ and the partially unfolded forms through a thermal intermediate containing an increased α-helix fraction (Figure 12).

Other protein forms of the Ser-32-Grb2-N-SH3 domain were observed by CD spectrometry. These include the molten globule resulting from the heating/cooling cycle of the native form and the nonnative all-$\beta$ form obtained from the α/$\beta$ form after addition of submicellar SDS (Figure 12). Interestingly, the CD spectra of the native SH3 domains from spectrin (*46*) and Sem-5 (*28*) are similar to that of this nonnative all-$\beta$ form form. Both the nonnative all-$\beta$ form and molten globule resemble the native form in that they do not contain α-helix and have a similar global $\beta$-content. However, they differ from the native form by a less condensed binding site, making the binding to proline-rich segments slightly less efficient ($K_{app} \approx 15-20$ $\mu$M, as indicated by CD measurements). In other words, the nonnative all-$\beta$ form and the molten globule have a nativelike secondary structure, with non-native tertiary contacts. Upon the assumption that, as in the case of the SH3 domain from α-spectrin (*48*), the native state may be not unique but rather composed of conformations where specific regions are able to undergo independent local folding/unfolding events, the nonnative all-$\beta$ form and, to some extent, all the molten globule-like forms could contribute to the conformational ensemble defining the native state. This is supported by the fact that both forms share the ability to revert to the native form in the presence of salt (Figure 12).

Considering the double mutant Y7V/C32S, the overall pattern is roughly the same. The observed conformations are similar to those of the C32S mutant but their distribution along the energy scale differs. This is probably associated

with the destabilization induced by the point mutation. Thus, the native form is not predominant at pH = 4.8, in the absence of salt, but rather is in equilibrium with the partially unfolded form. Similarly, the α/β form is not unique at pH = 8.2, but it is accompanied by a nonnative all-β form.

Along the free energy scale, two ensembles of potentially interconverting conformations are therefore observed, depending on the extent of their structural differences with the native conformation. The first ensemble consists of nonnative conformations with a nativelike secondary structure, but without critical tertiary contacts. The second is composed of more or less partially unfolded conformations, including α-helix or turnlike motifs in a nonnative secondary structure. Interestingly, all these conformations exist in mild or nondenaturing conditions. They probably have a compact inner structure, depending on the strength of nonlocal interactions, but only the native one possesses a condensed protein exterior, appropriate for the proline-rich peptide binding. These observations are in line with current understanding of the properties of partially unfolded proteins existing in nondenaturing conditions (*49*), and those of protein intermediates in the folding processes (*50*, *51*). From a thermodynamic point of view, the multiplicity of the conformations adopted by the Grb2N-SH3 domain is certainly related to its instability. As elsewhere suggested (*52*, *53*), the presence of partially unfolded exchanging forms could be physiologically relevant to intracellular regulatory processes involving the Grb2 adapter protein.

*Proline-rich Peptide Complex*. The native all-β conformation of the Grb2 N-SH3 domain was earlier shown, from NMR results (*9*), to be selectively involved in the binding to the VPPPVPPRRR decapeptide at neutral pH. With the aim of assessing by CD spectroscopy the possible structural changes resulting from this binding, we have assumed in a first approach that the native all-β conformation does not undergo any structural change upon binding. Consequently, below 220 nm, the estimated CD spectrum of the bound decapeptide was found to be similar to that of a left-handed PP-II helix, characterizing the ordered conformation of polyproline peptides at low temperatures (*54*, *55*). This type of helical conformation is also partially adopted by proline-rich peptides bound to SH3 domains at ambient temperature (*55*, *56*). However, at longer wavelengths, the CD spectrum estimated for the bound SH3 domain displays a broad positive band centered at 228 nm, whose intensity is too high to satisfactorily match the profile of a PP-II helix. This suggests that our initial assumption is not fully valid and that a limited structural change probably occurs within the native form of the SH3 domain upon binding. This may concern the tertiary contacts involving the tyrosine residues. This suggestion is supported by the formation of an exciton, which may result from an improved dipole−dipole interaction between the phenolic rings of Tyr-7 and Tyr-52. In the native conformation of the free SH3 domain, the spectral contribution of this exciton is hardly detectable because of the nearly perpendicular geometry of the two phenolic rings, as indicated by NMR (*9*). In contrast, the insertion of the Pro-2′ residue from the decapeptide into the binding pocket including the Tyr-7 and Tyr-52 residues likely entails a limited rearrangement of the phenolic rings. Consequently, the interaction of the aromatic dipoles may be significantly enhanced in the complex.

Taken together, our data suggest that the formation of the complex between the decapeptide and the SH3 domain is probably accompanied by two concerted reactions. The first is a significant folding of the proline-rich peptide, probably with a preference for the peptide part, which closely contacts the SH3 domain, as previously shown for the SH3 domain from PI3 kinase (*56*). The second reaction is a local conformational change within a hydrophobic pocket in the binding site of the native conformation of the SH3 domain.

Finally, it must be kept in mind that binding was studied with an isolated proline-rich peptide, which does not rigorously mimic the interaction between the SH3 domain and the protein in which the peptide is included. This was pointed out for the binding of the SH3 domain from Abl or from Fyn tyrosine kinase to the Nef protein in the conserved core of HIV-1 (*57*). Thus, a hydrophobic interaction between the protein structure proximal to the proline-rich region and the RT loop adjacent to the binding site in the SH3 domain results in a greater binding affinity (*58*). Such a phenomenon might be pertinent to the binding of the Grb2 N-SH3 domain to the C-terminal tail of Sos.

## ACKNOWLEDGMENT

We are indebted to Professor F. Pattus (CNRS UPR 9050) for cordial hospitality, use of his dichrograph, and for helpful advice in interpretation of CD data. We thank Dr. F. Cornille and Mme. C. Lenoir for their help in the synthesis of SH3 domains and proline-rich peptide, and Dr. K. Takeda for careful reading of the manuscript and are also grateful to P. Chassard and D. Wagner for valuable technical assistance.

## REFERENCES

1. Pawson, T., and Schlessinger, J. (1993) *Curr. Biol. 3*, 434−442.
2. Marshall, C. J. (1994) *Curr. Opin. Genet. Dev. 4*, 82−89.
3. Yu, H., Rosen, M. K., Shin, T. B., Seidel-Duggan, C., Brugge, J. S., and Shreiber, S. L. (1992) *Science 258*, 1665−1668.
4. Musacchio, A., Gibson, T., Lehto, V. P., and Saraste, M. (1992) *FEBS Lett. 307*, 55−61.
5. Morton, C. J., Pugh, D. J. R., Brown, E. L. J., Kahmann, J. D., Renzoni, D. A. C., and Campbell, I. D. (1996) *Structure 4*, 705−714.
6. Pawson, T. (1995) *Nature 373*, 573−580.
7. Kuriyan, J., and Cowburn, D. (1997) *Annu. Rev. Biophys. Biomol. Struct. 26*, 259−288.
8. Musacchio, A., Noble, M., Pauptit, R., Wierenga, R., and Saraste, M. (1992) *Nature 359*, 851−855.
9. Goudreau, N., Cornille, F., Duchesne, M., Parker, F., Tocqué, B., Garbay, C., and Roques, B. P. (1994) *Nat. Struct. Biol. 1*, 898−907.
10. Teresawa, H., Kohda, D., Hatanaka, H., Tsuchiya, S., Ogura, K., Nagata, K., Ishii, S, Mandiyan, V., Ullrich, A., Schlesinger, J., and Inagaki, F. (1994) *Nat. Struct. Biol. 1*, 891−897.
11. Wittekind, M., Mapelli, C., Lee, V., Goldfrab, V, Friedrichs, M. S., Meyers, C. A., and Mueller, L. (1997) *J. Mol. Biol. 267*, 933−952.
12. Toudmadje, A., Alcorn, S. W., and Johnson, C., Jr. (1992) *Anal. Biochem. 200*, 321−331.
13. Provencher, S. W. (1982) *Comput. Phys. Commun. 27*, 213−227 and 229−242.
14. Kahn, P. C. (1979) *Methods Enzymol. 61*, 339−378.
15. Manalavan, P., and Johnson, W. C., Jr. (1987) *Anal. Biochem. 167*, 76−85.
16. Yang, J. T., Wu, C.-S. C., and Martinez, H. M. (1986) *Methods Enzymol. 130*, 208−269.
17. Chakrabartty, A., Kortemme, T., Padmanabhan, S., and Baldwin, L. (1993) *Biochemistry 32*, 5560−5565.

18. Manning, M. C., and Woody, W. (1989) *Biochemistry 28*, 8609−8613.
19. Manning, C. M., Illangasekare, M., and Woody, R. W. (1988) *Biophys. Chem. 31*, 77−86.
20. Yang, J. J., Pitkeathly, M., and Radford, S. E. (1994) *Biochemistry 33*, 7345−7353.
21. Chang, C. T., Wu, C. S. C., and Yang, J. T. (1978) *Anal. Biochem. 91*, 12−31.
22. Kuwajima, K. (1989) *Proteins: Struct. Funct. Genet. 6*, 87−103.
23. Pace, C. N. (1986) *Methods Enzymol. 131*, 266−280.
24. Myers, J. K., Pace, C. N., and Scholtz, J. M. (1995) *Protein Sci. 4*, 2138−2148.
25. Kalnin, N. N., and Kuwajima, K. (1995) *Proteins: Struct., Funct., Genet. 23*, 163−176.
26. Logan, T. M., Theriault, Y., and Fesik, S. W. (1994) *J. Mol. Biol. 236*, 637−648.
27. Clark, S. G., Stern, M. J., and Horowitz, H. R. (1992) *Nature 356*, 340−344.
28. Lim, W. A., Fox, R. O., and Richards, F. M. (1994) *Protein Sci.* 3, 1261−1266.
29. Manning, C., and Woody, R. W. (1991) *Biopolymers 31*, 569−586.
30. Rabanal, F., Ludevid, M. D., Pons, M., and Giralt, E. (1993) *Biopolymers 33*, 1019−1028.
31. Strickland, E. H. (1974) *CRC Crit. Rev. Biochem. 2*, 113−175.
32. Tinoco, I., Jr. (1963) *Radiat. Res. 20*, 133−139.
33. Vidal, M., Goudreau, N., Cornille, F., Cussac, D, Gincel, E., and Garbay, C. (1999) *J. Mol. Biol. 290* (3), 717−730.
34. Goudreau, N. (1995) Thèse de doctorat de l'Université René Descartes, Paris.
35. Farrow, N. A., Zhang, O., Forman-Kay, J. D., and Kay, L. E. (1995) *Biochemistry 34*, 868.
36. Zhang, O., and Forman-Kay, J. D. (1995) *Biochemistry 34*, 6784−6794.
37. Zhang, O., and Forman-Kay, J. D. (1997) *Biochemistry 36*, 3959−3970.
38. Mok, Y.-K, Kay, C. M., Kay, L. E., and Forman-Kay, J. (1999) *J. Mol. Biol. 289*, 619−638.
39. Martinez, J. C., Pisabarro, M. T., and Serrano, L. (1997) *Nat. Struct. Biol. 5*, 721−729.
40. Hennesey, J. P., Jr., and Johnson, W. C., Jr. (1981) *Biochemistry 20*, 1085−1094.
41. Barrow, C. J., Yasuda, A., Kenny, P. T. M., and Zagorski, M. G. (1992) *J. Mol. Biol. 225*, 1075−1093.
42. Grantcharova, V. P., and Baker, D. (1997) *Biochemistry 36*, 15685−15692.
43. Viguera, A. R., Jimenez, M. A., Rico, M., and Serrano, L. (1996) *J. Mol. Biol. 255*, 507−521.
44. Clark, P. L., Liu, Z. P., Rizo, J., and Gierash, L. M. (1997) *Nat. Struct. Biol. 4* (11), 883−886.
45. Chen, Y.-J., Lin, S.-C., Tzeng, S.-R., Patel, H. V., Lyu, .P−C. and Cheng, J.−W. (1996) *Proteins: Struct., Funct., Genet. 26*, 465−471.
46. Viguera, A. R., Martinez, J. C., Filimonov, V. V., Mateo, P. L., and Serrano, L. (1994) *Biochemistry 33*, 2142−2150.
47. Guijarro, J. I., Sunde, M., Jones, J.A., Campbell, I.D., and Dobson, C. M. (1998) *Proc. Natl. Acad. Sci. U.S.A. 95* (8), 4224−4228.
48. Sadqi, M., Casares, S., Abril, M. A., López-Mayorga, O., Conejero-Lara, F., and Freire, E. (1999) *Biochemistry 38*, 8899−8906.
49. Prieto, J., Wilmans, M., Jimenez, M. A., Rico, M., and Serrano, L. (1997) *J. Mol. Biol. 268*, 760−778.
50. Shortle, D., Wang, Y., Gillespie, J. R., and Wrabl, J. O. (1996) *Protein Sci. 5*, 991−1000.
51. Wrabl, J. O., and Shortle, D., (1996) *Protein Sci. 5*, 2343−52.
52. Pace, C. N. (1990) *Trends Biochem. Sci. 15*, 14.
53. Arfin, S. M., and Bradshaw, R. A. (1988) *Biochemistry 27*, 7979.
54. Renzoni, D. A., Pugh, D. J. R., Siligardi, G., Das, P., Morton, C. J., Rossi, C., Waterfield, M. D., Campbell, I. D., and Ladbury, J. E. (1996) *Biochemistry 35*, 15646−15653.
55. Siligardi, G., and Drake, A. F. (1995) *Biopolymers 37*, 281−292.
56. Yu, H., Chen, J. K., Feng, S., Dalgarno, D. C., Brauer, A. W., and Schreiber, S. L. (1994) *Cell 76*, 933−945.
57. Ren, R., Mayer, B. J., Cicchetti, P., and Baltimore, D. (1993) *Science 259*, 1157−1161.
58. Lee, C.-H., Saksela, K., Mirza, A., Chait, B. T., and Kuriyan, J. (1996) *Cell 85*, 931−942.


BI9929103